Acid–Induced Changes in Thermal Stability and Fusion Activity of Influenza Hemagglutinin

6 AUTHORS, INCLUDING:

David P. Remeta

Rutgers, The State University of New Jersey

40 PUBLICATIONS **904** CITATIONS

SEE PROFILE

Conceicao Minetti

Rutgers, The State University of New Jersey

54 PUBLICATIONS **648** CITATIONS

SEE PROFILE

Anu Puri

National Institutes of Health

72 PUBLICATIONS **2,680** CITATIONS

SEE PROFILE

Robert Blumenthal

National Institutes of Health

271 PUBLICATIONS **11,863** CITATIONS

SEE PROFILE

Acid-Induced Changes in Thermal Stability and Fusion Activity of Influenza Hemagglutinin

David P. Remeta,[‡,§] Mathias Krumbiegel,[‖,⊥] Conceição A. S. A. Minetti,[‡,§] Anu Puri,[‖] Ann Ginsburg,[‡] and Robert Blumenthal*[‖]

Section on Protein Chemistry, Laboratory of Biochemistry, National Heart, Lung, and Blood Institute, National Institutes of Health, 50 South Drive, Room 2339, Bethesda, Maryland 20892-8012, and Laboratory of Experimental and Computational Biology, National Cancer Institute−FCRDC, National Institutes of Health, Building 469, Room 211, Frederick, Maryland 21702

ABSTRACT: The conformational and thermal stability of full-length hemagglutinin (HA) of influenza virus (strain X31) has been investigated using a combination of differential scanning calorimetry (DSC), analytical ultracentrifugation, fluorescence, and circular dichroism (CD) spectroscopy as a function of pH. HA sediments as a rosette comprised of 5−6 trimers (31−35 S) over the pH range of 7.4−5.4. The DSC profile of HA in the native state at pH 7.4 is characterized by a single cooperative endotherm with a transition temperature (T_m) of 66 °C and unfolding enthalpy (ΔH_{cal}) of 800 kcal·(mol of trimer)$^{-1}$. Upon acidification to pH 5.4, there is a significant decrease in the transition temperature (from 66 to 45 °C), unfolding enthalpy [from 800 to 260 kcal·(mol of trimer)$^{-1}$], and $\Delta H_{cal}/\Delta H_{vH}$ ratio (from 3.0 to ∼1.3). Whereas the far- and near-UV ellipticities are maintained over this pH range, there is an acid-induced increase in surface hydrophobicity and decrease in intrinsic tryptophanyl fluorescence. The major contribution to the DSC endotherm arises from unfolding HA1 domains. The relationship between acid-induced changes in thermal stability and the fusion activity of HA has been examined by evaluating the kinetics and extent of fusion of influenza virus with erythrocytes over the temperature and pH range of the DSC measurements. Surprisingly, X31 influenza virus retains its fusion activity at acidic pH and temperatures significantly below the unfolding transition of HA. This finding is consistent with the notion that the fusion activity of influenza virus may involve structural changes of only a small fraction of HA molecules.

Hemagglutinin (HA)[1] is the influenza virus glycoprotein responsible for the binding of the virus to sialic acid containing receptors on target cells and for fusion of viral and target membranes (*1*). The fusion is triggered by acid-induced conformational changes of HA (*2, 3*) that occur in the low-pH environment of the endosomes (*4*). As a result, the viral nucleocapsid complex is transferred into the cell, and viral replication is initiated. HA is a trimeric integral membrane protein (M_r 220 000) comprised of an ectodomain of identical subunits, each of which contains two polypeptides, HA1 and HA2, linked by a disulfide bond (*5*). HA1 is

the receptor-binding subunit, and HA2 is responsible for the fusogenic activity of HA (*1*).

Structural information is available for the ectodomains of both the native protein at neutral pH (*5*) and a portion of HA2 (i.e., TBHA2) following exposure to low pH (*6*). The glycine-rich NH$_2$ terminal (residues 1−20) region of HA2 has been designated as the fusion peptide based on a variety of genetic, protein chemical, and biophysical studies (*7*). In the native trimeric HA structure at neutral pH, the three fusion peptides adopt sequential reverse turn conformations and are partially buried between α-helices at the interface between the HA2 and HA1 subunits, near the viral side of the ectodomain stalk (*5*). Activation of HA at low pH results in extensive molecular rearrangements leading to extrusion of the fusion peptide from this buried location, whereupon it can interact with the target and/or viral membrane (*1*). Determination of the HA structure in the activated, low-pH state has been hindered by the exposure of the hydrophobic fusion peptide, which causes disordered aggregation of the trimers in aqueous solution. However, the high-resolution structure of a stable truncated recombinant ectodomain of the fusion-pH conformation of HA2, which lacks the N-terminal fusion peptide, has been determined at 1.9 Å resolution (*8*). According to this structure, the N- and C-terminal residues of the molecule form an N cap, terminating both the N-terminal α-helix and the central coiled-coil.

---

* Address correspondence to this author at National Cancer Institute−FCRDC, Building 469, Room 216A, Frederick, MD 21702. TEL: 301-846-1446; FAX: 301-846-6192; E-Mail: blumen@helix.nih.gov.

‡ National Heart, Lung, and Blood Institute.

§ Present address: Department of Chemistry and Chemical Biology, Rutgers−The State University of New Jersey, 610 Taylor Rd., Piscataway, NJ 08854.

‖ National Cancer Institute−FCRDC.

⊥ Present address: Oberhof 24, 06254 Zoeschen, Germany.

[1] Abbreviations: HA, hemagglutinin purified from influenza virus strain X31; HA1 and HA2, disulfide-linked subunits of HA; BHA, bromelain digested hemagglutinin (minus the C$_2$-terminal anchor peptide); CD, circular dichroism spectroscopy; DSC, differential scanning calorimetry; CR, cooperative ratio of the calorimetric to the van't Hoff enthalpy changes; Nile Red, a phenoxazine dye (Molecular Probes, Eugene, OR); R18, octadecyl rhodamine (Molecular Probes, Eugene, OR); TBHA2, thermolysin digested BHA2.

Comparison with the crystal structures of a number of other membrane fusion-inducing proteins reveals common structural motifs (*9*), which suggest potential mechanisms for membrane fusion. The most plausible scenario is that activation of the fusion protein results in release of the fusion peptide and extension of a central coiled-coil structure (*6, 10*). The new positioning of the fusion peptides at the tip of the stalk provides for easy contact with the target cell membrane. A small group of proximal fusion proteins that are simultaneously inserted into both the viral and target membranes constitute a potential fusion site (*11*).

To better understand the unfolding pathways HA negotiates when triggered to promote fusion, we have assessed the conformational and energetic stability of full-length HA in solution as a function of pH, utilizing a combination of calorimetric, spectroscopic, and analytical centrifugation techniques. Previous studies regarding the thermal stability of HA as a function of pH have been based on spectroscopic measurements and limited proteolysis (*12−14*) using either the whole virus or solubilized fragments (BHA and TBHA2). However, no systematic evaluation of the energetics of unfolding purified full-length HA has thus far been obtained. This multiparametric approach facilitates elucidation of the HA unfolding pathway including the population of intermediate states while assessing the energetics of the unfolding process. Information gleaned from this study provides insight into the mechanisms of pH-induced conformational changes, thereby improving our understanding of HA-mediated fusogenic activity in virus-infected mammalian cells.

EXPERIMENTAL PROCEDURES

Virus Preparation. Influenza virus (strain X31) was prepared as described previously (*15*). Briefly, the virus was grown at 37 °C for 48 h in the allantoic cavity of 10-day-old embryonated hen eggs. The allantoic fluid of the eggs was collected and the cell debris removed by a low-speed spin (1000*g*) for 30 min. The virus was pelleted by centrifuging the allantoic fluid at 95000*g* for 60 min. The supernatant was discarded and the pellet resuspended in PBS buffer (137 mM NaCl, 2.7 mM KCl, 8.1 mM Na_2HPO_4, 1.5 mM KH_2PO_4, pH 7.4) and homogenized at 4 °C with a Teflon-coated homogenizer.

Viral Fusion Activity Assay. Purified X31 influenza virus was labeled with octadecyl rhodamine (R18) as described (*16*). Unincorporated dye was removed by passage through a PD-10 (Sephadex G-25 M) column using PBS as the elution buffer. R18-labeled X31 was collected in the void volume (≈0.5 mg of virus/mL), stored at 4 °C in the dark, and used within 24 h. Human erythrocyte ghosts were prepared essentially as described (*17*) and resuspended at a concentration of ≈5 × 10⁹ ghosts/mL in PBS. To allow association of virus with the ghosts, a mixture of ghosts and R18-labeled X31 influenza virus (0.2 mL of each) was incubated at room temperature for 15−20 min with occasional shaking. Following addition of 1 mL of PBS, the unbound virus was removed by centrifugation at 6000 rpm for 2 min in a microcentrifuge.

The pellet was resuspended in 1 mL of PBS, stored on ice, and used within 1−2 h for fusion experiments. Fusion kinetics were monitored at preset pH and temperature values as described (*16*). Variations in the pH values between 25

and 45 °C were ≤0.1 unit. Percent fusion at a given time was calculated as follows: $100 × [(F − F_o)/(F_t − F_o)]$, where F_o, F, and F_t are the fluorescence values at zero, a given time, and in the presence of Triton X-100, respectively.

Purification of Hemagglutinin. Viral membranes were solubilized in PBS containing 1.5% octyl-β-glucoside (Boehringer Mannheim, Indianapolis, IN) and agitated on a rotating shaker for 1 h at 4 °C. The insoluble material was removed by centrifugation at 100000*g* for 60 min. The supernatant containing hemagglutinin in detergent micelles was purified by affinity chromatography on a ricin A column (Sigma Chemical Corp., St. Louis, MO) in accordance with established procedures (*3*). The protein was eluted from the ricin column by the addition of 0.2 M D-galactose to the PBS−detergent buffer system. Samples were dialyzed at 4 °C with a minimum of two 2.0 L changes over a period of 48 h to ensure complete removal of octyl-β-glucoside and galactose. The purity of hemagglutinin was assessed by SDS−PAGE employing 12% TRIS−glycine gradient gels under both reducing and nonreducing conditions.

Preparation of Hemagglutinin Solutions. Concentrated stock solutions of purified HA were dialyzed against a mixed buffer system comprised of 50 mM sodium phosphate, 50 mM sodium acetate, 100 mM NaCl, and 1.0 mM Na-EDTA (pH 7.4), hereafter designated as Buffer A. The latter was preferred to phosphate-buffed saline for its buffering capacity over a broad temperature and pH range. The dialyzed samples were diluted to an appropriate concentration based upon the sensitivity requirements of the technique to be used. The temperature of the HA solutions was maintained at 4.0 °C for pH adjustments. Microliter aliquots of 1 M acetic acid dissolved in the appropriate buffer were added dropwise to each HA sample with constant stirring to ensure homogeneous mixing and to minimize exposure of HA to conditions of extreme acidity. HA at pH 7.4 in Buffer A was also dialyzed versus an identical buffer containing 1% octyl-β-glucoside (Buffer B). All HA solutions were incubated at 37 °C for 30 min and cooled to 4 °C prior to calorimetric, ultracentrifugation, and spectroscopic analysis. Protein concentration was determined either by the BioRad assay (using bovine serum albumin as a standard and adjusted for carbohydrate content) and/or by UV absorption spectrophotometry employing a specific absorbance of $A_{280nm,1cm} = 1.25$ cm³/mg. The latter was calculated from the amino acid composition and a trimer molecular weight of 220 000 which includes 19% carbohydrate by weight (*5*).

Analytical Ultracentrifugation. A Beckman Optima model XL-A analytical ultracentrifuge equipped with a four-place AN-Ti rotor was used for sedimentation velocity experiments, with overnight preequilibration of the rotor to the desired temperature. The density of each dialysate buffer was determined at 20.00 °C with a Paar DMA 58 densitometer, and the relative viscosity was measured as described previously (*18*): Buffer A: $\eta/\eta_0 = 1.0589$; $\rho_{20} = 1.01140$; Buffer B: $\eta/\eta_0 = 1.0766$; $\rho_{20} = 1.01245$. Protein samples (0.34 mL) were loaded into the right side of each 4° Kel-F-coated double-sector centerpiece, and appropriate reference buffers (0.35 mL) were placed in each left sector in 12 mm cells, equipped with plane UV-quartz windows. In the absence of detergent, three cells were run simultaneously at 25 000 rpm while scanning in a continuous mode (0.003 cm step) with triple averaging at 280 nm at 6 or 7

min intervals, after equilibration and radial calibration at 3000 rpm at which speed radial and wavelength (9−11 averages at 1 nm resolution) scans were collected. A speed of 35 000 rpm was used for HA in 1% octyl-β-glucoside at pH 7.4. A. P. Minton's TRACKER program (http://bbri-www.eri.harvard.edu/RASMB/rasmb.htm1) was used to monitor the progress of runs. Sedimentation coefficients (s_{obs}) were calculated by the radial derivative method (XLAVEL) from Beckman Instruments, Inc., and corrected to values corresponding to the density and viscosity of water at 20.00 °C using a partial specific volume of 0.73 mL/g for HA for the buoyancy factor ($s_{20,w}$). The value of 0.73 mL/g for the partial specific volume of HA rosettes was estimated by sedimentation equilibrium (*19*), in which 0.100 mL of HA ($A_{280nm} \sim$ 0.3) in aqueous and D_2O buffers was simultaneously sedimented at 3700 rpm at 4.0 °C until concentration gradients were time-independent (between 48 and 72 h). Prior to centrifugation, HA samples ($\sim$1 mg/mL) were dialyzed extensively versus either aqueous or D_2O buffers containing 50 mM sodium phosphate, 100 mM NaCl, 1.0 mM Na-EDTA with $\sim$4−8 mM acetic acid (added as glacial acetic acid) for pH (pD) adjustment to pH 7.2 (pD = 7.6) using H_2O or D_2O (99.9 atom % D from Sigma) to prepare buffers.

Circular Dichroism Spectroscopy. Acid-induced changes in the secondary and tertiary structure of hemagglutinin (mean residue molecular weight of 111.7) were evaluated by circular dichroism (CD) spectroscopy in the far-UV (190−250 nm) and near-UV (250−350 nm) regions, respectively. Spectra of samples containing 0.1−1.0 mg/mL protein were recorded at 0.1 nm wavelength intervals on a JASCO model 710 circular dichroism spectropolarimeter (JASCO Inc., Easton, MD) employing a scan speed of 10 nm/min and average response time of 1 s. A minimum of four consecutive scans were accumulated and the average spectra stored. The temperature of the samples was maintained at 37 °C through the use of water-jacketed cylindrical quartz cuvettes interfaced to a NESLAB model RTE-111 water bath regulated by an in-line temperature probe at the outlet of the cell. Path lengths of either 0.01 cm (far-UV) or 1.0 cm (near-UV) were employed for isothermal studies.

An AVIV model 62A DS circular dichroism spectrometer (AVIV Instruments USA, Lakewood, NJ) equipped with a programmable thermoelectrically controlled sample compartment was employed for temperature-dependent studies. The thermal stability of HA secondary structure was monitored by heating samples containing 100 μg/mL protein at a programmed rate of 90 °C/h over the range of 5−105 °C in a 0.1 cm quartz cuvette. The mean residue molar ellipticity at 222 nm was recorded at 0.1 °C intervals employing a time constant of 4 s.

Fluorescence Spectroscopy. Isothermal and temperature-dependent fluorescence spectra were acquired on an AVIV model ATF105 ratio spectrofluorometer (AVIV Instruments USA, Lakewood, NJ) equipped with programmable thermoelectrically controlled sample and reference compartments. Fluorescence spectra of samples containing 100 μg/mL protein were recorded over the range of 300−500 nm employing an excitation wavelength of 295 nm and slit widths of 2.5 nm. Temperature-dependent changes in intrinsic Trp fluorescence as a function of pH were monitored by heating the samples at a programmed rate of 90 °C/h over the range of 5−95 °C. The fluorescence emission intensity

at 345 nm was recorded at 0.1 °C intervals employing a time constant of 4 s.

Acid-induced changes in the exposure of HA hydrophobic residues were estimated by measuring the fluorescence of samples incubated with Nile Red (Molecular Probes, Eugene, OR) in accordance with an established protocol (*20*). Samples containing 50 μg/mL of protein at the desired pH were incubated in the presence of 0.1 μg/mL Nile Red at 37 °C for 30 min prior to measurement. Nile Red fluorescence measurements were performed on an SLM AMINCO−Bowman 8100 Series 2 spectrofluorometer. Temperature stability was maintained through use of a water-jacketed 1.0 cm quartz cuvette interfaced to a programmable NESLAB RTE-111 water bath. Fluorescence spectra were recorded over the range of 560−650 nm employing an excitation wavelength of 550 nm and slit widths of 5 nm. The fluorescence emission intensity of Nile Red at 610 nm was monitored as a function of pH at 37 °C.

Differential Scanning Calorimetry (DSC). DSC experiments were performed on MicroCal MC-2 and VP-DSC calorimeters (MicroCal LLC, Northampton, MA) and a Nano-DSC calorimeter (Calorimetry Sciences Corp., Spanish Fork, UT). DSC data were corrected for the instrument baseline, normalized for a scan rate of 90 °C/h and protein concentration based on a trimer M_r of 220 000 (*5*), and the excess heat capacity was expressed in kcal·K^{-1}·(mol of trimer)$^{-1}$, where 1.000 cal = 4.184 J. Data conversion and analysis were performed using Origin software (MicroCal LLC, Northampton, MA) and the EXAM program (*21*). A sigmoidal baseline (EXAM) between pre- and post-transition regions was subtracted from each endotherm in order to calculate the area, which is equal to the unfolding enthalpy (ΔH_{cal}). The corresponding van't Hoff enthalpy (ΔH_{vH}) is estimated from $\Delta H_{vH} = 4.00RT_m^2(C_{p,m}/\Delta H_{cal})$ (*22*), where R is the gas constant [1.987 kcal/(mol·K)], the ratio $C_{p,m}/\Delta H_{cal}$ represents the maximum peak height to the area of the transition, and T_m is the transition temperature in degrees kelvin at $C_{p,m}$. The cooperative ratio (CR) is defined by the relation: CR = $\Delta H_{cal}/\Delta H_{vH}$ and used to estimate the number of unfolding domains.

RESULTS

Hydrodynamic Properties. Sedimentation velocity experiments have been performed to verify protein homogeneity as well as to characterize the hydrodynamic behavior of HA preparations. The results presented in Table 1 indicate that in the absence of detergent or a target membrane, HA adopts a characteristic rosette assembly, sedimenting as a spherical complex of five to six trimers (31, 35 S). These results are consistent with electron microscopy studies of intact influenza virus in which rosette structures of five to six trimers are observed (*23*). Except where indicated otherwise in Table 1, HA sediments as a single component (i.e., symmetrical boundary) as monitored at 280 nm with loading absorbances of 0.6−1.0. However, boundary spreading analysis suggests that some heterogeneity in particle size exists, specifically as a function of temperature. For example, sedimentation coefficients ($s_{20,w}$) of 35 S are measured for HA at 20 °C at either pH 7.4 or pH 5.85, whereas at 5 °C, values of $s_{20,w}$ are 31 S for HA at pH 7.4, 5.85, and 5.4. Temperature may therefore be a factor in the size of rosette structures observed.

Table 1: Sedimentation Coefficients of Influenza Virus Hemagglutinin under Different Experimental Conditions[a]

pH	T_{run} (°C)	s_{obs} (S ± 0.3)	$s_{20,w}$ (S)	species present[b]
7.4	20.0	33.6	35	rosette
5.85	20.0	33.1	35	rosette
7.4	5.0	19.7	31	rosette
5.85	5.0	18.1	30	rosette
5.4	5.0	19.5	31	rosette
5.4/7.4[c]	5.0	19.7	31	rosette
5.4	20.0	28.0	31	rosette[d]
7.4 (1% OG)	20.0	9.2	10.3	trimer

[a] Sedimentation coefficients (observed s, corrected to the viscosity and density of water at 20 °C, $s_{20,w}$) in Svedberg units (S) are reported as average values for two to four different preparations of hemagglutinin (HA) in Buffer A adjusted to the indicated pH, preincubated for 30 min at 37 °C, and cooled prior to ultracentrifugation (25 000 rpm for rosettes or 35 000 rpm for trimer in the presence of octyl-β-glucoside) at the indicated temperature. Except where indicated otherwise, HA sediments as a single boundary as monitored at 280 nm with loading absorbances of 0.6−1.0. [b] Five to six trimers of HA per rosette (31−35 S) in the absence of 1% OG and monomeric trimer (10 S) in the presence of 1% OG (see text). [c] HA sample incubated at pH 5.4 for 30 min at 37 °C, cooled to 4 °C, and immediately reneutralized to pH 7.4 prior to ultracentrifugation. [d] Some instability (i.e., time-dependent aggregation) of HA at pH 5.4 evident during centrifugation at 20 °C, although the major component sedimented at 31 S.

Assuming the relationship $M_1/M_2 = (s_1/s_2)^{3/2}$ and a shape factor similar to that of dodecameric glutamine synthetase from *E. coli*, which has $s_{20,w} = 20.3$ S and $M_r = 622 000$ (*18*, *24*), $s_{20,w}$ values of 31 and 35 S for HA in the absence of detergent correspond to molecular weights between 1.2 and 1.4×10^6, indicating ~5−6 trimers of HA per rosette complex.

All the samples analyzed in Table 1 have been preincubated at the indicated pH for 30 min at 37 °C and then cooled to the appropriate temperature prior to sedimentation velocity experiments. The fact that the rosettes pretreated at pH 5.4 and 37 °C are stable during the 5 °C run with an $s_{20,w}$ value of 31 S is consistent with the observation that influenza virus, pretreated at pH 5.4 and 37 °C for periods as long as 1 h, retains both fusogenic activity and typical spike morphology (*25*). Although X31 influenza virus does not exhibit fusion activity at pH 5.4 and 20 °C, HA does mediate fusion at pH 5.4 and 35 °C (see Figure 5C). When the pH 5.4 and 37 °C treated samples are sedimented at 20 °C, both dissociated (trimer) and aggregated (rosette) species are evident, indicating that the preparations of HA become unstable when exposed for lengthy periods of time at pH 5.4 and 20 °C. The onset of this instability correlates well with the fusogenic activity of HA and its susceptibility to inactivation.

In the presence of 1% octyl-β-glucoside, HA sediments as a homogeneous species with $s_{20,w} = 10.3$ S (Table 1). This $s_{20,w}$ value corresponds to a trimer M_r of 220 000 ± 10 000, using the above relationship with glutamine synthetase as the reference protein. From these data, a frictional ratio (f/f_0) of 1.28 is calculated, which corresponds to an axial ratio of ~5 for a prolate ellipsoid. Sedimentation equilibrium experiments with HA in 1% octyl-β-glucoside are complicated by the presence of the detergent due to micelle formation (*26*), and consequently cannot be analyzed reliably. Nevertheless, the sedimentation velocity results reveal a trimeric structure for HA at pH 7.4 in the presence of 1% octyl-β-glucoside. This is in general agreement with previous observations of Doms and Helenius (*27*), who estimated a

sedimentation coefficient of 9.0 S by sucrose density gradient centrifugation of HA in detergent at 20 °C. Uncorrected sedimentation coefficients of 9 S for BHA at neutral pH in the absence or presence of detergent as well as 30 S for the BHA rosette at pH 5.0 have been measured previously (*28*) by sucrose density gradient centrifugations at 20 °C.

A Stokes radius of ~95 Å is calculated for a rosette of six HA trimers from the data obtained at 20 °C (Table 1), which clearly is an underestimate based on the structural information available. Crystallographic structures of BHA have shown that at neutral pH, trimeric BHA adopts a cylindrical structure with a length of 135 Å and radius of 30 Å, or an axial ratio of 4.5 (*5*), whereas these dimensions at low pH are 165×25 Å (*6*). Trimer lengths of 205 and ~187 Å for intact HA at pH 7.0 in detergent and rosette structures, respectively, have been measured in electron microscopy studies (*23*), that report a hydrodynamic radius of ~170 Å for BHA rosettes from small-angle neutron scattering experiments. In view of our sedimentation data, it is apparent that the HA surface domains in rosettes exert minimal frictional drag during sedimentation.

Secondary and Tertiary Structure. Secondary and tertiary structures of HA have been examined by far- and near-UV circular dichroism spectra at 37 °C as a function of pH. The far-UV CD spectrum of HA at pH 7.4 is characteristic for an α-helical-containing protein with minima observed at 208 and 222 nm. The overall secondary structure of HA in rosettes is maintained throughout the pH range studied (i.e., pH 7.5−4.5) as depicted in Figure 1A, in agreement with previous findings (*29*). The near-UV CD remains unchanged in the pH range of 7.4−5.4, below which it undergoes gradual disruption with a transition midpoint centered at pH ~5.1 (Figure 1A). The kinetics of the tertiary structure changes have been monitored by near-UV CD (*30*) and by intrinsic Trp fluorescence (*31*), revealing that the pH-dependent changes are complete within ~30 min at 37 °C, at which time changes in tertiary structure are irreversible. Since most of the aromatic residues are located predominantly in the ectodomain of HA (*29*), the observed reduction in the near-UV CD spectrum may correlate with losses in the environmental asymmetry upon acidification. The apparent disruption of tertiary structure as HA is acidified below pH 5.4 in this study (Figure 1A) reflects the instability of HA when incubated at 37 °C and low pH, an observation that is consistent with the sedimentation velocity experiments (Table 1). Our CD measurements therefore reveal that acidification of HA in rosettes from pH 5.4 to 4.9 significantly disrupts tertiary structure with minimal perturbation of secondary structure.

Hydrophobicity. Nile Red interactions as a function of pH have been performed to assess the surface hydrophobicity of HA upon exposure to acidic conditions. The pH-dependent changes in hydrophobicity have been monitored by titrations with the apolar fluorescent probe Nile Red, which is uncharged and well suited for pH-dependent changes in protein conformation (*20*). The acid-induced increase in protein hydrophobic group exposure as monitored by Nile Red binding to HA (reflected by fluorescence increases at 610 nm) indicates that protonation of HA induces conformational changes that result in increased exposure of hydrophobic residues that bind to Nile Red (Figure 1B). A transition midpoint at pH 5.4 is consistent with hydrophobic
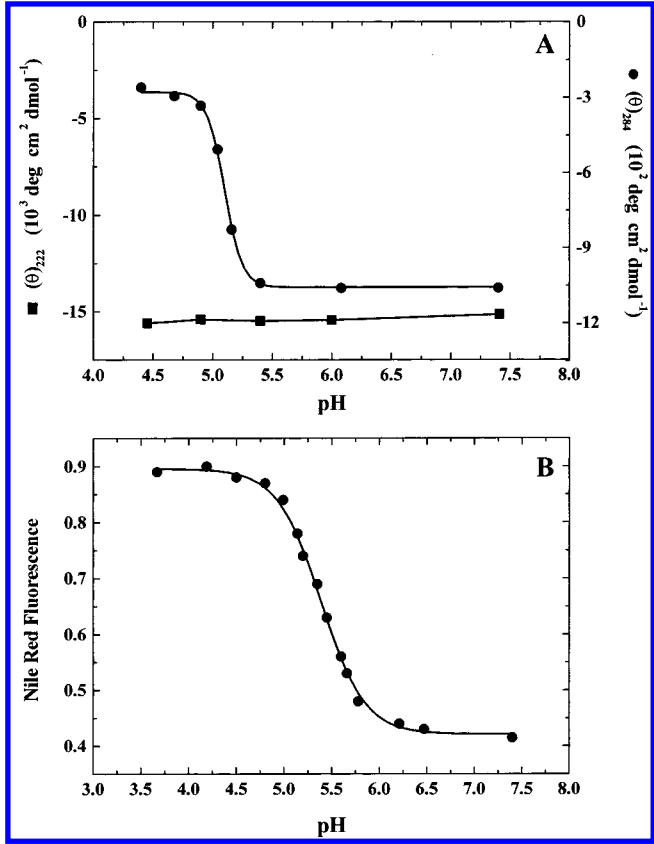
FIGURE 1: (A) Stability of HA secondary and tertiary structure as a function of pH at 37 °C. The mean residue ellipticities at 222 nm (circles) and 284 nm (squares) are plotted vs pH. Sample concentrations are 0.10 mg/mL HA for far-UV and 1.0 mg/mL HA for near-UV determinations. (B) Hydrophobicity changes of HA rosettes monitored as a function of pH at 37.0 °C. The pH-dependent change in the fluorescence emission intensity of Nile Red is monitored at 610 nm (550 nm excitation wavelength).

residue exposure upon acidification. Similar changes in the hydrophobicity of HA upon acidification have been revealed by binding to liposomes (*3*) and changes in 1,1′-bis(4-anilino)naphthalene-5,5′-disulfonic acid fluorescence (*32*). The acid-induced increase in Nile Red fluorescence at 610 nm does not change significantly with time (data not shown).

Conformational Stability of HA at Neutral pH. The conformational stability of HA has been investigated by differential scanning calorimetry (DSC) to characterize thermodynamically the structural changes accompanying the unfolding process. The thermal stability of HA either in the presence or in the absence of detergent has been assessed by DSC the heat capacity changes associated with unfolding HA in its trimeric form or associated as rosettes, respectively. At pH 7.4, the DSC profile is characterized by a single cooperative endotherm (Figure 2, upper profile, closed circles represent HA in rosettes) centered at a transition temperature of 66 °C with a cooperative ratio (CR) = 3.0 and an observed enthalpy change of 800 kcal·(mol of trimer)$^{-1}$. A scan rate of 90 °C/h has been used since slower scan rates induce post-transition aggregation that decreases the reliability of post-transition baselines. Inspection of the DSC profile for HA at pH 7.4 reveals that post-transition points decrease somewhat more rapidly than predicted from the fit of the data (solid line) to a model for three independent two-state unfolding transitions, whereas pre-transition and transition
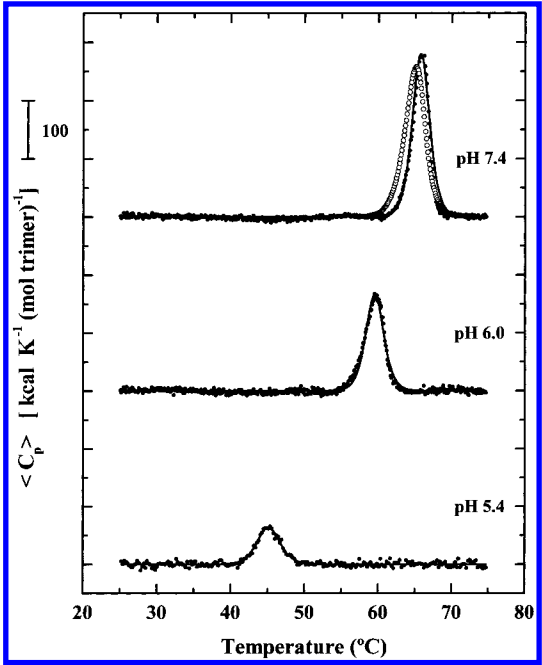

FIGURE 2: Thermal unfolding of HA as a function of pH. DSC endotherms of HA rosettes at pH 7.4, 6.0, and 5.4 in the absence (closed circles) of detergent. The fit of the data in each case to a two-state model with the number of unfolding domains treated as a variable (CR in Table 2) is represented by the solid line. The endotherms are corrected for buffer baseline, normalized for scan rate and protein concentration, and then pre- and post-transition baselines subtracted. The open circles at pH 7.4 are the endotherm obtained for HA trimer in the presence of 1.0% octyl-β-glucoside.

Table 2: Summary of DSC Parameters for Thermal Unfolding of HA as a Function of pH in the Absence and Presence of 1% Octyl-β-glucoside[a]

pH	T_m (°C)	ΔH_{cal} (kcal/mol)	ΔH_{vH} (kcal/mol)	CR	CR × ΔH_{vH} (kcal/mol)
7.4	65.8	800	292	3.0	880
7.0	66.2	809	290	3.0	870
6.5	63.6	748	300	2.5	760
6.2	59.6	600	254	2.3	580
6.0	59.5	528	269	2.0	540
5.7	52.5	365	183	2.0	370
5.4	45.2	260	195	1.3	250
5.0	42.2	76	101	1.0	100
7.4 (1% OG)	65.0	785	255	3.0	770

[a] Purified hemagglutinin rosettes (0.25−1.0 mg/mL) dialyzed against Buffer A (50 mM sodium phosphate, 50 mM sodium acetate, 100 mM NaCl, 1 mM Na-EDTA), adjusted to the indicated pH, and incubated for 30 min at 37 °C prior to each DSC experiment (rows 1−8). In row 9, HA at pH 7.4 dialyzed against Buffer A containing 1% octyl-β-glucoside (1% OG) is a trimer. DSC scans are from 15 to 85 °C at a scan rate of 90 °C/h, and in all cases, a single endotherm is observed and analyzed. After subtraction of the instrument baseline, DSC data are normalized for scan rate (1.5 K/min) and protein concentration using a trimer M_r = 220 000 and a specific absorbance at 280 nm of 1.25 cm^2/mg. CR is the cooperative ratio defined as $\Delta H_{cal}/\Delta H_{vH}$, where ΔH_{cal} is equal to the area of the observed endotherm and $\Delta H_{vH} = 4RT^2$(area/$C_{p,max}$). Errors in T_m are ±0.2 °C and in ΔH_{cal} are ±10%. Discrepancies between ΔH_{cal} values and values of CR × ΔH_{vH} are due to post-transition aggregation (refer to endotherms in Figure 3).

data fit this model of unfolding. This indicates that some aggregation of unfolded domains occurs at neutral pH. For this reason, Table 2 includes a column of values for the product (i.e., CR × ΔH_{vH}) which in some cases represent higher estimates of the enthalpy changes for HA unfolding

than that obtained from direct integration of the total area for each endotherm (ΔH_{cal}). Thus, comparison of the ΔH_{cal} value to the product (CR $\times$ ΔH_{vH}) reveals those cases in which post-transition aggregation may be responsible for decreasing the observed area of the endotherm.

In the presence of 1% octyl-β-glucoside at pH 7.4 (open circles in Figure 2), the DSC endotherm of the HA trimer is nearly identical to that of the rosette. In fact, the T_m is only ~1 °C lower than that for HA in the absence of detergent, which suggests that the protein is only slightly stabilized against thermal unfolding in the rosette. The enthalpy change for unfolding HA in 1% OG (CR $\times$ ΔH_{vH}) is ~100 kcal/mol lower than that for HA in the rosette at pH 7.4, although the ΔH_{cal} values are similar due to post-transition aggregation of HA in rosettes, resulting in a decrease in the apparent area. Furthermore, the cooperative ratios of unfolding the HA trimer in the presence or absence of detergent are essentially identical. A value for ΔC_p of 7 $\pm$ 1 kcal K^{-1} mol^{-1} is estimated for HA in 1% OG.

Thermal Unfolding of Protonated HA Conformational States. The thermal stability of HA rosettes is markedly decreased upon acidification from pH 7.4 (T_m = 66 °C) to pH 5.4 (T_m = 45 °C). The decrease in transition temperatures during acidification most likely results from the disruption of HA1−HA1 contacts within the trimer and HA1−HA2 contacts in the stem region. Since the HA1 domains have been reported to dissociate and remain globular with rearranged tertiary structure upon acidification (*33*), the decrease in cooperativity ratio suggests that the globular heads interact during unfolding. The middle and lower endotherms in Figure 2 show DSC endotherms for HA rosettes at pH 6.0 and 5.4, respectively. As the pH is decreased, the width of the DSC transition increases, and the area of the respective endotherm approaches that of ΔH_{vH}. The pH-induced changes are irreversible as demonstrated by reneutralizing an HA sample initially incubated at pH 5.4, and observing identical DSC profiles with T_m = 45 °C (data not shown). A value for ΔC_p of 7.1 $\pm$ 1 kcal K^{-1} mol^{-1} for the thermal unfolding of HA in rosette structures is estimated from the enthalpy change per domain as a function of T_m at each pH (*34*). This value is consistent with the ΔC_p estimated from fits of pre- and post-transition baselines of DSC endotherms for HA rosettes (data not shown) and detergent-solubilized trimers.

Temperature-Dependent Tryptophan Exposure. The thermal stability of HA tertiary structure has been assessed by monitoring temperature-induced changes in the intrinsic tryptophanyl fluorescence as a function of pH. In the native state at pH 7.4, the fluorescence spectrum of HA reflects the characteristic apolar environment of the aromatic residues comprising the HA1 and HA2 domains, each of which contains six Trp residues. Acidification of HA in rosette structures results in the exposure of these aromatic residues that may be monitored by observing the decrease in the intrinsic tryptophanyl fluorescence. It is important to distinguish between the acid-induced conformational changes of HA that result in increased Trp exposure versus the temperature-dependent changes in Trp exposure at a particular pH. The isothermal decrease in fluorescence intensity as a function of pH at 37 °C has been presented in one of our earlier studies (*31*). Temperature-induced changes in intrinsic Trp residue fluorescence of HA in rosettes at pH
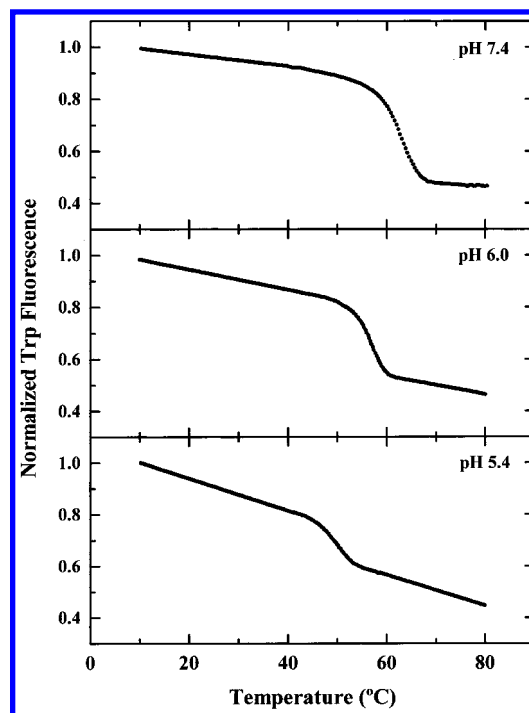

FIGURE 3: Effect of pH on the temperature-induced exposure of Trp residues. Progress curves for temperature-induced changes in the intrinsic tryptophanyl fluorescence for HA rosettes at pH 7.4, 6.0, and 5.4. Fluorescence intensity changes at 345 nm (with excitation at 295 nm) are normalized relative to the fluorescence intensity at 5.0 °C.

7.4, 6.0, and 5.4 are presented in Figure 3. These profiles are normalized relative to the fluorescence intensity at 5 °C to facilitate direct comparison of the thermally induced changes in amplitude as a function of pH. The transition temperatures of 63 and 57 °C for Trp residue exposure at pH 7.4 and 6.0 are somewhat lower than the respective T_m values determined from DSC at these pH values (Table 2). However, the transition temperature of 50 °C for Trp exposure at pH 5.4 is higher than the T_m value from DSC, and may reflect interactions among HA domains during unfolding at low pH. Upon acidification to pH 5.0, there is no evidence of additional Trp residue exposure, and the HA melting profile solely reflects the temperature dependence of intrinsic Trp fluorescence (data not shown). The approximate correlation observed between the Trp fluorescence melting profiles and the DSC endotherms at each pH suggests that temperature-induced unfolding of HA reflects disruption of residual domain contacts within HA1 and HA2, resulting in exposure of buried Trp residues.

Thermal Stability of Secondary Structure. Temperature-dependent perturbations in secondary structure have been assessed for both the native (pH 7.4) and low-pH (pH 5.4) conformations of HA by monitoring changes in the mean residue molar ellipticity at 222 nm. Figure 4A presents far-UV CD spectra acquired at 5.0 °C (solid line) and 95.0 °C (dashed line) for HA rosettes at neutral pH. Inspection of the temperature progress curve (Figure 4A, inset) reveals that the native conformation of HA is thermally stable at temperatures below 60 °C. The secondary structure is only slightly perturbed upon heating to 100 °C with the transition at ~65 °C characterized by the partial unfolding of less than 10% of secondary structure elements. Consequently, the
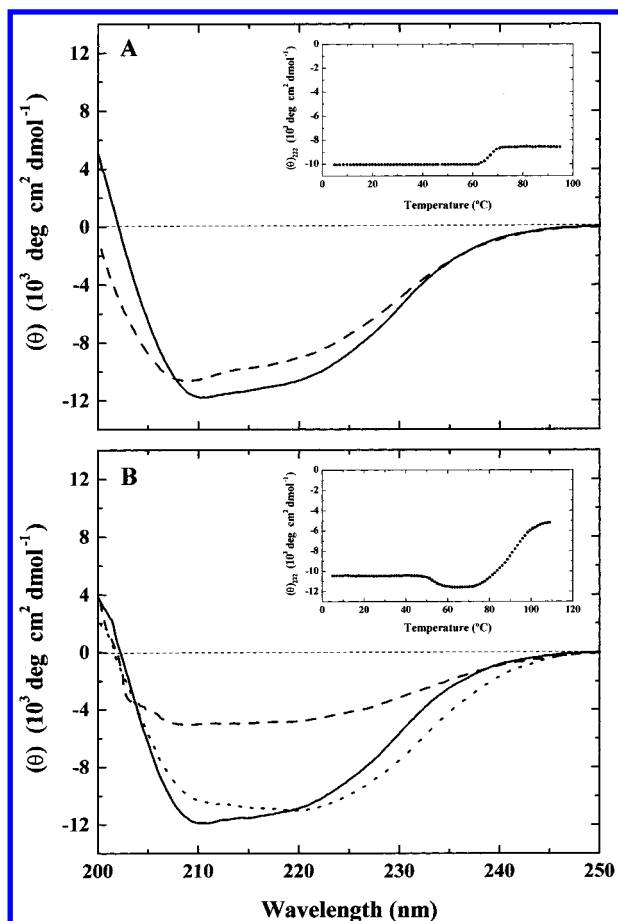
FIGURE 4: Thermal stability of HA secondary structure as monitored by temperature-dependent changes in the far-UV CD. (A) Spectra of 0.10 mg/mL HA rosettes at 5 °C (solid line) and 95 °C (dashed line) at pH 7.4. (B) Spectra of 0.10 mg/mL HA rosettes at 5 °C (solid line), 65 °C (dotted line), and 110 °C (dashed line) at pH 5.4. Progress curves for temperature-induced changes in mean residue ellipticity at 222 nm are shown as insets for HA in panels A (pH 7.4) and B (pH 5.4).

thermal stability of secondary structure in the native state contrasts with the temperature-dependent increase in tryptophan exposure (Figure 3) as well as the magnitude of excess heat capacity changes in DSC (Table 2). There is a significant decrease in the thermal stability of secondary structure of the low-pH conformation as noted by comparing the far-UV CD spectra recorded at 5.0 °C (solid line), 65.0 °C (dotted line), and 110.0 °C (dashed line) in Figure 4B. The temperature progress curve (Figure 4B, inset) is characterized by a biphasic transition which suggests there is some thermally induced ordering and rearrangement of secondary structure at ~53 °C, followed by thermal disruption and unfolding of secondary structure at ~90 °C. Comparison of the low and neutral pH states therefore reveals significant differences in the thermal stability and overall loss of HA secondary structure.

Temperature and pH Dependence of Viral Fusion Activity.
To relate the low-pH-induced changes in thermal stability with the fusion activity of influenza hemagglutinin, we measured fusion of influenza virus X31 with erythrocyte membranes as a function of pH and temperature. The kinetics and extent of fusion of the X31 strain with a variety of targets have been reported previously using assays for continuous monitoring of fluorescence changes (*31, 35−37*). However,

a complete temperature−pH profile starting at 5 °C is not available in the literature. To monitor fusion with biological membranes, we have performed a fluorescence dequenching assay that utilizes the lipophilic fluorescent dye octadecyl rhodamine B (R18) incorporated into intact virions under self-quenching conditions (*38*). Once fusion has occurred, the fluorophore diffuses into the larger target, resulting in relief of self-quenching, and consequently an increase in the fluorescence signal is observed.

Fluorescence changes in R18 as a result of fusion have been measured spectrofluorometrically with a 1s time resolution as a function of pH at temperatures between 5 and 55 °C. Figure 5A shows a typical set of kinetic curves at 35 °C. Whereas at pH values above 5.8 we observe no R18 dequenching at this temperature, we note that at pH 5.8 the fusion reaction starts increasing after about 200 s following exposure of the virus−cell complexes to low pH and 35 °C. This lag time decreases between pH 5.8 and 5.0, and at pH 5.0, it is not measurable with the time resolution employed. The rate of fluorescence change increases markedly over the same pH range. We have previously interpreted the lag time as reflecting the relative rates of rearrangements of lipids into the fusogenic state following acid-induced conformational changes in HA (*31, 37, 39*). Accordingly, higher amounts of HA activation will result in decreased lag times and faster fusion kinetics (*37*). The delay time for a population of cells represents the earliest time point at which lipid continuity is discerned for a subpopulation of our fusing species, with a total dequenching above the noise of our experiment. Operationally, the delay time can be defined as the intersection of the time axis with the tangent drawn to the steepest part of the fusion curve (*40*). To determine the kinetic parameters governing HA-mediated fusion at a given pH and temperature, we have fit the kinetic data to an empirical equation from which we have derived the time at which the rate of fusion is maximal (t_{max}), which is closely related to the delay time (*40*). In Figure 5B we have plotted the t_{max} as a function of pH for three temperatures, and derived pH values where fusion activity attains its half-maximal level ($pH_{1/2}$) of 5.35, 5.50, and 5.67 at 25, 35, and 45 °C, respectively.

At temperatures below 25 °C, we could not obtain reliable fits to our kinetic data throughout the pH range studied. We therefore used the extent of fusion after 400 s to obtain a complete pH profile in the temperature range from 5 to 55 °C. Figure 5C shows the extent of fusion after 400 s at three representative temperatures. As indicated above, X31 influenza virus exhibits negligible fusion activity at pH 5.4 and 20 °C, whereas HA does mediate fusion at pH 5.4 and 35 °C As shown in Figure 5C, the $pH_{1/2}$ shifts as a function of temperature from $pH_{1/2} = 4.88$ at 10 °C, to $pH_{1/2} = 5.18$ at 20 °C, to $pH_{1/2} = 5.45$ at 35 °C. This temperature is significantly below the transition temperature measured for thermal unfolding of HA rosettes at that pH (e.g., $T_m = 45.2$ °C at pH 5.4; see Table 2). A complete profile of the $pH_{1/2}$ values for the extent of fusion between 5 and 55 °C and for the t_{max} between 25 and 55 °C for X31 influenza virus fusion activity is presented in Figure 5D. In the temperature range where we could determine both the kinetics and extent of fusion, the $pH_{1/2}$ values at a given temperature appear comparable. In Figure 5D, we have also plotted the T_m values as a function of pH from our DSC experiments in Table 2.
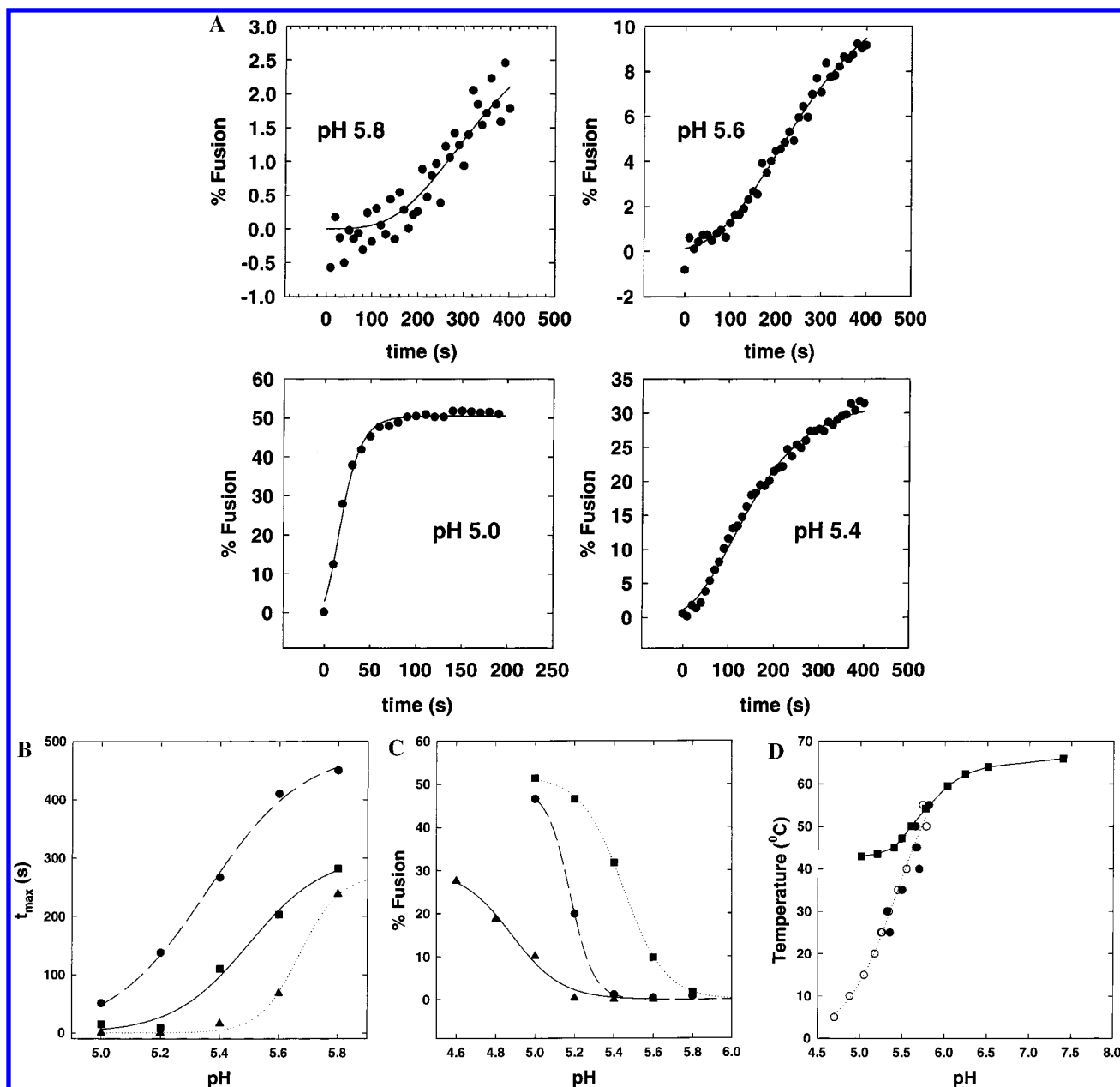
FIGURE 5: Comparison of the temperature and pH dependence of viral fusion activity of HA with transition temperatures (T_m) obtained for thermal unfolding of HA by DSC. (A) Kinetics of X31 influenza fusion at 35 °C and pH 5.8 (top left panel), pH 5.6 (top right panel), pH 5.4 (bottom right panel), and pH 5.0 (bottom left panel). The data were collected with 1 s time resolution, but for clarity only 10 s data points are shown. The kinetic data have been fit to a variety of sigmoidal functions provided by the SigmaPlot2000 (SPSS Science, Chicago, IL) function library. The "Gompertz" equation ($f = a*\exp[-\exp(-(x - x_0)/b)]$) provided the best fit to the full set of curves. In this equation, x_0 is the time at which the rate of fusion is maximal (t_{max}), which is closely related to the delay time. (B) Values of t_{max} derived from curves such as shown in (A) as a function of pH at 25 (●), 35 (■), and 45 °C (▲), respectively. The lines represent best fits to the equation: $f = a/\{1 + \exp[-b(pH - pH_{1/2})]\}$, yielding $pH_{1/2}$ values of 5.35, 5.50, and 5.67 at 25, 35, and 45 °C, respectively. (C) Extent of fusion after 400 s as a function of pH at 10 (▲), 20 (●), and 35 °C (■), respectively. The lines represent best fits to the equation: $f = a/\{1 + \exp[-b(pH - pH_{1/2})]\}$, yielding $pH_{1/2}$ values of 4.88, 5.18, and 5.45 at 10, 20, and 35 °C, respectively. (D) $pH_{1/2}$ at a given temperature derived from t_{max} values (●) of curve fits such as those shown in (A) and (B), and from extent of fusion values (○) derived from curve fits such as those shown in (C). (■) represent T_m values as a function of pH derived from DSC measurements in Table 2.

The data in Figure 5D clearly indicate that X31 fusion activity is elicited at temperatures significantly below the unfolding transition of influenza HA.

DISCUSSION

The structure of the extracytoplasmic domain of HA is comprised of two distinct regions, namely, a fibrous stem containing residues from HA1 and HA2, and a globular region composed solely of HA1 residues arranged in an eight-stranded β-structure (5). A significant number of residues within the HA2 subunits adopt a triple-stranded α-helical coiled-coil that stabilizes HA trimeric structure. HA1 globular subunits also associate into a trimeric assembly, and the N- and C-terminal regions of HA1 participate in long-range interactions with HA2 in the stem region. Our hydrodynamic studies confirm that the full-length protein adopts a trimeric structure in the presence of detergent (Table 1). Removal of the detergent via dialysis facilitates reas-

sembly of HA into rosette structures comprised of 5–6 trimers, in agreement with previous studies (*23*). We find that these rosettes are stable in the native (pH 7.4) state and after pretreatment at 37 °C and pH 5.4. The onset of rosette instability (pH < 5.4) appears to correlate well with the viral fusion activity (Figure 5).

The widely accepted "spring-loaded" type of mechanistic model for HA-mediated fusion posits that the cleaved HA is a metastable intermediate in which extensive contacts between HA1 and HA2 kinetically trap the molecule behind a free-energy barrier (*1, 6, 10*). Application of an acidic trigger surmounts the barrier to yield a stable low-pH conformation of HA2. The observation that the bacterial-expressed ectodomain of HA2, comprising amino acids 23–185, folds spontaneously at neutral pH into the fusion-pH-induced conformation (*13*) is consistent with this notion. Nevertheless, our temperature-dependent calorimetric and spectroscopic measurements indicate that intact HA exhibits significant conformational and thermal stability at neutral pH. DSC profiles at pH 7.4 reveal a single endotherm that is characterized by a transition temperature (T_m) of 66.0 °C and an unfolding enthalpy (ΔH_{cal}) of 800 kcal/mol (Figure 2). A specific enthalpy change of 4.2 cal g^{-1} at 37 °C (based on ΔC_p = 7.1 kcal K^{-1} mol^{-1}) indicates that HA only undergoes partial thermal unfolding (30–50%). The ratio of the calorimetric to van't Hoff enthalpies is a measure of the number of cooperative domains that undergo unfolding and provides insight into the magnitude of interdomain interactions within multidomain proteins (*34, 41*). Cooperative ratios greater than unity are indicative of a non-two-state process and may therefore reveal the presence of unfolding intermediates. Evaluation of the $\Delta H_{cal}/\Delta H_{vh}$ ratio for the HA endotherm at neutral pH indicates that three domains of comparable stability unfold independently. Significantly, deconvolution analysis of the HA endotherm at pH 7.4 reveals that the data fit a model of three independent two-state unfolding transitions (data not shown). Evidence for three cooperative unfolding domains is consistent with the structural model of HA in the native state (*5*). Furthermore, binding of monoclonal antibodies at neutral pH to epitopes in the interfacial region (site D) suggests relative movement of the HA1 globular domains, which is consistent with the notion that these domains unfold independently (*42*).

Extensive studies have been performed on the acid-triggered conformational changes that are related to the fusogenic activity of influenza HA (*2*). White and Wilson (*43*) have probed the details of the pH-dependent conformational changes in X31 HA using a panel of anti-HA-peptide antibodies. The results of their study indicate that the acid-triggered conformational change of isolated HA occurs in at least two steps: the fusion peptide comes out of the trimer interface ("intermediate state") followed by dissociation of the globular heads ("the low pH form"). The intermediates are also characterized by susceptibility to proteinase K digestion and binding to liposomes (*3, 15*). Although these intermediates may actually consist of a population of states, for convenience we will refer to these as the "intermediate state". Upon acidification to the optimal pH for fusogenic activity at 37 °C, long-range contacts between HA1 interfaces are disrupted, as indicated by

changes in spike morphology (*15, 25, 44*) and reactivity to anti-peptide antibodies raised against the top and interface regions (*43*). Pretreatment of X31 virus under these conditions leads to inactivation of HA-mediated fusion (*15, 25*). Significantly, at pH values below 5.0, preincubation of HA at 37 °C results in temperature-dependent calorimetric and spectroscopic profiles that are indistinguishable from the baseline. By contrast, in the intermediate state, HA maintains its spike morphology and fusogenic activity (*25*). These results support the notion that during fusion, overall HA structural integrity is preserved. The near-UV CD spectra reveal states below pH 5.4, in which the tertiary structure is disrupted with a transition midpoint at pH 5.1 (Figure 1A). In contrast, the secondary structure remains intact throughout the entire pH range (pH 7.4 to pH 4.5). The low-pH form has significant secondary structure but is devoid of most tertiary structure contacts. In this state, the triple-helical coiled-coil structure is retained together with the transmembrane segments, thereby preserving the overall trimeric assembly. The acid-induced conformational changes resulting in the loss of HA1/HA1 and HA1/HA2 contacts within the trimer without major changes in secondary structure are consistent with studies on low-pH HA2 that is characterized by an overall retention of secondary structure content, although it lacks approximately two-thirds of the molecule including the HA1 subunit (*6, 29*).

The DSC endotherms of HA rosettes pretreated at 37 °C and acid pH are characterized by a thermodynamic domain that unfolds less cooperatively (i.e., broader transition) and exhibits a reduced enthalpy and lower transition temperature relative to the neutral pH conformation (Figure 2). Inspection of the relative pH dependent decrease in enthalpy per domain as a function of temperature reveals a linear relationship which is entirely consistent with previous studies conducted on a large number of proteins (*22*) and demonstrates that the pH-dependent enthalpy changes are a reflection of the reduction in denaturation temperatures. Acidification of HA from pH 7.4 to pH 5.4 not only decreases the transition temperature of unfolding but also reduces the cooperative ratio from 3.0 to 1.3 (Table 2). The observed reduction in CR as a function of pH suggests that exposed hydrophobic residues in thermally labile HA1 domains interact during denaturation and the collapsed structure unfolds as a single cooperative unit with some heterogeneity indicated by broader endotherms. Our temperature-dependent far-UV CD studies reveal discrete changes in which the neutral pH state exhibits a transition midpoint at 65 °C that is characterized by no more than a 10% decrease in molar ellipticity (Figure 4). In contrast to the high thermal stability of the native conformation at pH 7.4, a significant temperature-dependent reduction in secondary structure (∼60%) occurs at low pH, albeit at much higher temperature (T_m ∼ 90 °C). The thermally unfolded low-pH form is therefore characterized by a loss of tertiary structure (T_m = 45 °C) with subsequent disruption of approximately two-thirds of the secondary structure at a transition temperature of 90 °C. This high-temperature transition is not detected calorimetrically as it lacks the cooperativity characteristic of tertiary contacts and therefore resembles the unfolding of compact denatured states reported for other proteins (*45*) that lack tertiary structure but retain significant secondary structure.

We find that the $pH_{1/2}$ values for t_{max} or extent of fusion after 400 s vary with temperature (Figure 5). These data are consistent with Wharton et al. (*35*), who reported for WT X31 a difference of 0.89 pH unit between the $pH_{1/2}$ values at 5 and 50 °C, whereas we observe a difference of 1.07 pH units between these temperatures (Figure 5D). For temperatures above 55 °C, the virus−erythrocyte complexes are unstable, and therefore the fusion measurements are unreliable. Using an X31 mutant virus that has a higher pH threshold for triggering conformational changes, it is possible to observe fusion at lower temperatures and pH values closer to neutral (*14, 35*). The fusion experiments reported in this study have been performed employing the same batch of influenza virus and an identical assay at all temperature and pH values, and the DSC measurements have been conducted using purified HA extracted from this batch of influenza virus. The most striking observation in our study is that X31 influenza virus retains its fusion activity at acidic pH and temperatures significantly below the unfolding transition temperature of HA (Figure 5). This implies either that the entire population of HA molecules does not require a great deal of unfolding to induce fusion (*15, 25, 46−48*) or that only an undetectable fraction of HA molecules needs to unfold to induce fusion. Studies showing that HA-mediated fusion requires both separation of the globular head domains (*49, 50*) and loop to helix transitions of HA2 residues (*6, 10, 51*) indicate a requirement for major structural changes in the HA molecules mediating fusion. The hypothesis that fusion activity of influenza virus may involve structural changes of a small fraction of HA molecules is consistent with the notion that only a few HA molecules are involved in the fusion process (*39, 52−54*).

REFERENCES

1. Skehel, J. J., and Wiley, D. C. (2000) *Annu. Rev. Biochem. 69*, 531−569.
2. Wiley, D. C., and Skehel, J. J. (1987) *Annu. Rev. Biochem. 56*, 365−394.
3. Doms, R. W., Helenius, A., and White, J. (1985) *J. Biol. Chem. 260*, 2973−2981.
4. Marsh, M., and Helenius, A. (1989) *Adv. Virus Res. 36*, 107−151.
5. Wilson, I. A., Skehel, J. J., and Wiley, D. C. (1981) *Nature 289*, 366−373.
6. Bullough, P. A., Hughson, F. M., Skehel, J. J., and Wiley, D. C. (1994) *Nature 371*, 37−43.
7. Durell, S. R., Martin, I., Ruysschaert, J. M., Shai, Y., and Blumenthal, R. (1997) *Mol. Membr. Biol. 14*, 97−112.
8. Chen, J., Skehel, J. J., and Wiley, D. C. (1999) *Proc. Natl. Acad. Sci. U.S.A. 96*, 8967−8972.
9. Skehel, J. J., and Wiley, D. C. (1998) *Cell 95*, 871−874.
10. Carr, C. M., and Kim, P. S. (1993) *Cell 73*, 823−832.
11. Weissenhorn, W., Dessen, A., Calder, L. J., Harrison, S. C., Skehel, J. J., and Wiley, D. C. (1999) *Mol. Membr. Biol. 16*, 3−9.
12. Ruigrok, R. W., Martin, S. R., Wharton, S. A., Skehel, J. J., Bayley, P. M., and Wiley, D. C. (1986) *Virology 155*, 484−497.
13. Chen, J., Wharton, S. A., Weissenhorn, W., Calder, L. J., Hughson, F. M., Skehel, J. J., and Wiley, D. C. (1995) *Proc. Natl. Acad. Sci. U.S.A. 92*, 12205−12209.
14. Carr, C. M., Chaudhry, C., and Kim, P. S. (1997) *Proc. Natl. Acad. Sci. U.S.A. 94*, 14306−14313.
15. Puri, A., Booy, F., Doms, R. W., White, J. M., and Blumenthal, R. (1990) *J. Virol. 64*, 3824−3832.
16. Puri, A., Clague, M. J., Schoch, C., and Blumenthal, R. (1993) *Methods Enzymol. 220*, 227−287.
17. Herrmann, A., Clague, M. J., Puri, A., Morris, S. J., Blumenthal, R., and Grimaldi, S. (1990) *Biochemistry 29*, 4054−4058.
18. Shapiro, B. M., and Ginsburg, A. (1968) *Biochemistry 7*, 2153−2167.
19. Edelstein, S. J., and Schachman, H. K. (1967) *J. Biol. Chem. 242*, 306−311.
20. Sackett, D. L., and Wolff, J. (1987) *Anal. Biochem. 167*, 228−234.
21. Kirchhoff, W. H. (1993) NIST Technical Note 1401: EXAM (CODEN: NTNOEF), U.S. Government Printing Office, Washington, DC, Ref Type: Report.
22. Privalov, P. L., and Khechinashvili, N. N. (1974) *J. Mol. Biol. 86*, 665−684.
23. Ruigrok, R. W., Wrigley, N. G., Calder, L. J., Cusack, S., Wharton, S. A., Brown, E. B., and Skehel, J. J. (1986) *EMBO J. 5*, 41−49.
24. Ginsburg, A., and Zolkiewski, M. (1991) *Biochemistry 30*, 9421−9429.
25. Korte, T., Ludwig, K., Booy, F. P., Blumenthal, R., and Herrmann, A. (1999) *J. Virol. 73*, 4567−4574.
26. Shire, S. J. (1994) in *Modern Analytical Ultracentrifugation* (Schuster, T. M., and Laue, T. M., Eds.) pp 261−297, Birkhauser, Boston.
27. Doms, R. W., and Helenius, A. (1986) *J. Virol. 60*, 833−839.
28. Skehel, J. J., Bayley, P. M., Brown, E. B., Martin, S. R., Waterfield, M. D., White, J. M., Wilson, I. A., and Wiley, D. C. (1982) *Proc. Natl. Acad. Sci. U.S.A. 79*, 968−972.
29. Wharton, S. A., Ruigrok, R. W., Martin, S. R., Skehel, J. J., Bayley, P. M., Weis, W., and Wiley, D. C. (1988) *J. Biol. Chem. 263*, 4474−4480.
30. Korte, T., Ludwig, K., Krumbiegel, M., Zirwer, D., Damaschun, G., and Herrmann, A. (1997) *J. Biol. Chem. 272*, 9764−9770.
31. Krumbiegel, M., Herrmann, A., and Blumenthal, R. (1994) *Biophys. J. 67*, 2355−2360.
32. Korte, T., and Herrmann, A. (1994) *Eur. Biophys. J. 23*, 105−113.
33. Bizebard, T., Gigant, B., Rigolet, P., Rasmussen, B., Diat, O., Bosecke, P., Wharton, S. A., Skehel, J. J., and Knossow, M. (1995) *Nature 376*, 92−94.
34. Privalov, P. L. (1979) *Adv. Protein Chem. 33*, 167−241.
35. Wharton, S. A., Skehel, J. J., and Wiley, D. C. (1986) *Virology 149*, 27−35.
36. Stegmann, T., Hoekstra, D., Scherphof, G., and Wilschut, J. (1986) *J. Biol. Chem. 261*, 10966−10969.
37. Clague, M. J., Schoch, C., and Blumenthal, R. (1991) *J. Virol. 65*, 2402−2407.
38. Hoekstra, D., de Boer, T., Klappe, K., and Wilschut, J. (1984) *Biochemistry 23*, 5675−5681.
39. Blumenthal, R., Sarkar, D. P., Durell, S., Howard, D. E., and Morris, S. J. (1996) *J. Cell Biol. 135*, 63−71.
40. Bentz, J. (1992) *Biophys. J. 63*, 448−459.
41. Brandts, J. F., Hu, C. Q., Lin, L. N., and Mos, M. T. (1989) *Biochemistry 28*, 8588−8596.
42. Wiley, D. C., Wilson, I. A., and Skehel, J. J. (1981) *Nature 289*, 373−378.
43. White, J. M., and Wilson, I. A. (1987) *J. Cell Biol. 105*, 2887−2896.
44. Stegmann, T., Booy, F. P., and Wilschut, J. (1987) *J. Biol. Chem. 262*, 17744−17749.
45. Griko, Y. V., Freire, E., and Privalov, P. L. (1994) *Biochemistry 33*, 1889−1899.
46. Stegmann, T., White, J. M., and Helenius, A. (1990) *EMBO J. 9*, 4231−4241.
47. Shangguan, T., Siegel, D. P., Lear, J. D., Axelsen, P. H., Alford, D., and Bentz, J. (1998) *Biophys. J. 74*, 54−62.
48. Kanaseki, T., Kawasaki, K., Murata, M., Ikeuchi, Y., and Ohnishi, S. (1997) *J. Cell Biol. 137*, 1041−1056.

2054 *Biochemistry, Vol. 41, No. 6, 2002*

Remeta et al.

49. Godley, L., Pfeifer, J., Steinhauer, D., Ely, B., Shaw, G., Kaufmann, R., Suchanek, E., Pabo, C., Skehel, J. J., and Wiley, D. C. (1992) *Cell 68*, 635−645.
50. Kemble, G. W., Bodian, D. L., Rose, J., Wilson, I. A., and White, J. M. (1992) *J. Virol. 66*, 4940−4950.
51. Qiao, H., Pelletier, S. L., Hoffman, L., Hacker, J., Armstrong, R. T., and White, J. M. (1998) *J. Cell Biol. 141*, 1335−1347.

52. Danieli, T., Pelletier, S. L., Henis, Y. I., and White, J. M. (1996) *J. Cell Biol. 133*, 559−569.
53. Gunther-Ausborn, S., Schoen, P., Bartoldus, I., Wilschut, J., and Stegmann, T. (2000) *J. Virol. 74*, 2714−2720.
54. Bentz, J. (2000) *Biophys. J. 78*, 886−900.

BI015614A